

1 **Siberian Arctic black carbon: gas flaring and wildfire impact**

2
3 Olga B. Popovicheva¹, Nikolaos Evangeliou^{2,*}, Vasilii O. Kobelev³, Marina A. Chichayeva⁴,
4 Konstantinos Eleftheriadis⁵, Asta Gregorič^{6,7}, Nikolay S. Kasimov⁴

5
6 ¹ SINP, Lomonosov Moscow State University, 119991 Moscow, Russia

7 ² NILU - Norwegian Institute for Air Research, 2007 Kjeller, Norway

8 ³ Moscow Department of Russian Geographical Society, Moscow, Russia

9 ⁴ Geographical Department, Lomonosov Moscow State University, 119991 Moscow, Russia

10 ⁵ ERL, Institute of Nuclear and Radiological Science & Technology, Energy & Safety, N.C.S.R.
11 Demokritos, 15341 Attiki, Greece

12 ⁶ Aerosol d.o.o., SI-1000, Ljubljana, Slovenia

13 ⁷ Center for Atmospheric Research, University of Nova Gorica, SI-5270, Ajdovščina, Slovenia

14
15 * Corresponding authors: N. Evangeliou (Nikolaos.Evangeliou@nilu.no)

16
17

18 **Abstract**

19 As explained in the latest Arctic Monitoring and Assessment Programme (AMAP) report
20 released in early 2021, the Arctic has warmed three times more quickly than the planet as a whole,
21 and faster than previously thought. The Siberian Arctic is of great interest largely because
22 observations are sparse or largely lacking. A research aerosol station has been developed on the
23 Bely Island (Kara Sea) in Western Siberia. Measurements of equivalent black carbon (EBC)
24 concentrations were carried out at the “Island Bely” station continuously from August 2019 to
25 November 2020. The source origin of the measured EBC, and the main contributing sources were
26 assessed using atmospheric transport modelling coupled with the most updated emission
27 inventories for anthropogenic and biomass burning sources of BC.

28 The obtained climatology for BC during the period of measurements showed an apparent
29 seasonal variation with the highest concentrations between December and April (60 ± 92 ng/m³)
30 and the lowest between June and September (18 ± 72 ng/m³), typical of the Arctic Haze seasonality
31 reported elsewhere. When air masses arrived at the station through the biggest oil and gas
32 extraction regions of Kazakhstan, Volga-Ural, Komi, Nenets and Western Siberia, BC contribution
33 from gas flaring dominated over domestic, industrial, and traffic sectors, ranging from 47 to 68%,
34 with a maximum contribution in January. When air was transported from Europe during the cold
35 season, emissions from transportation were more important. Accordingly, shipping emissions
36 increased due to the touristic cruise activities and the ice retreat in summertime. Biomass burning
37 (BB) played the biggest role between April and October, contributing 81% at maximum in July.
38 Long-range transport of BB aerosols appeared to induce large variability to the Absorption
39 Ångström Exponent (AAE) with values ranging >1.0 (excluding outliers). As regards to the
40 continental contribution to surface BC at the “Island Bely” station, Russian emissions dominated
41 during the whole year, while European and Asian ones contributed up to 20% in the cold period.
42 Quantification of several pollution episodes showed an increasing trend in surface concentrations
43 and frequency during the cold period, as the station is directly in the Siberian gateway of the
44 highest anthropogenic pollution sources to the Russian Arctic.

45

46 **1 Introduction**

47 Global carbon pollution is annually produced by burning of fossil fuel and biomass.
48 Combustion emissions are increasingly recognized as an important source of chemically active
49 aerosols. Black carbon (BC) originates from the incomplete combustion of fossil fuels and biomass
50 burning; it is a short-lived climate forcer and absorbs incoming solar radiation and, therefore, is of
51 high significance for the Arctic climate (Wang et al., 2011). The combined total effects of BC and
52 sulfates cause an Arctic surface warming of +0.29°K explaining approximately 20% of the
53 observed Arctic warming since the early 1980s (Ren et al., 2020). BC resides in the lowest
54 atmospheric layer, affects aerosol-cloud interactions (Yun et al., 2013) and has a cloud and sea-
55 ice feedback when deposited (Flanner, 2013), thus accelerating melting (Quinn et al., 2008).

56 Long-range transport to the Arctic carries, among other aerosol constituents, many tracers
57 of anthropogenic and wildfire origin (Chang et al., 2011). (Winiger et al., 2016) showed that BC
58 in Arctic Scandinavia is predominantly linked to emissions in Europe. Over the whole Arctic
59 region (north of 66°N), Russia contributes 62% to surface BC (Zhu et al., 2020). Industrial and
60 residential sources are responsible for the highest measured BC concentrations at the Tiksi station
61 (Siberian Arctic) (Popovicheva et al., 2019b). (Stathopoulos et al., 2021) have demonstrated that
62 the long term impact of light absorbing carbon in the high Arctic is three times higher in the cold
63 period of the year compared to the warm period. There, fossil sources mostly prevail during winter-
64 spring season, while biomass burning sources dominate during low BC concentration periods in
65 summer (Winiger et al., 2017). Although BC dominates light absorption by atmospheric aerosols,
66 other carbonaceous aerosol species (brown carbon, BrC) represent an important fraction of light
67 absorption in the UV and near-UV spectrum, thus having an important role in the assessment of
68 radiative forcing in the Arctic climate. Spectral dependence of the light absorption is generally
69 described by the Absorption Ångström Exponent (AAE), which is typically used to differentiate
70 between aerosol types (BC, BrC) and sources of BC (Sandradewi et al., 2008; Helin et al., 2021;
71 Zotter et al., 2017).

72 Quantification of the particulate Arctic pollution is a serious problem worldwide; reliable
73 source emission inventories are challenged, and regional contributions of BC sources in the Arctic
74 are still inconclusive (Zhu et al., 2020). Global anthropogenic emission dataset ECLIPSEv6
75 (Evaluating the Climate and Air Quality Impacts of Short-lived Pollutants) using the GAINS
76 model (Klimont et al., 2017) includes all major economic sectors, such as energy and industrial
77 production, transport, residential combustion, agriculture, and waste, distinguishing between
78 sector-fuel-technology, fuels, and emission control options. The model predictions for European

79 gateway to the Arctic were greatly improved, when the emission inventory from anthropogenic
80 sources was updated by estimates of European BC emissions (Winiger et al., 2016).

81 Due to large size and continuous production, gas flaring of oil industry is one of the highest
82 BC emission sources (Ismail and Umukoro, 2012) with a strong environmental and climatic impact
83 for the Arctic (Cho et al., 2019). Flaring in ECLIPSEv6 dominates BC emissions in the Arctic;
84 models have found that flaring contributes 42% to the annual mean BC surface concentrations in
85 the Arctic (Stohl et al., 2013). However, because flares are difficult to measure, their particulate
86 emissions and physicochemical properties are still underestimated (Conrad and Johnson, 2017;
87 Popovicheva et al., 2019a). Currently, models are struggling to reproduce BC concentrations
88 largely due to emission-related uncertainties in the Arctic region (Schacht et al., 2019). The
89 observed annual mean contribution of fossil fuel combustion to the Arctic concentrations agrees
90 within a factor of two (Qi and Wang, 2019).

91 High latitude flaring emissions mainly originate from the North Sea, Norwegian Sea, the
92 northeastern part of European Russia (Komi Republic) and Western Siberia. The largest oil and
93 gas producing regions of northwestern Siberia are located along the main low-level pathway of air
94 masses entering the Arctic and thus have a disproportionately large contribution to the Arctic lower
95 troposphere (Stohl, 2006). (Eleftheriadis et al., 2009) and (Tunved et al., 2013) identified these
96 regions as a key source for the highest measured BC concentrations and sub-micrometer aerosol
97 mass concentrations, respectively, at the Zeppelin station. The impact of BC long-range transport
98 from northwestern Siberia was also observed at the Ice Base Cape Baranova station located on
99 Severnaya Zemlya archipelago (Eastern Siberia) (Manousakas et al., 2020). Accordingly, possible
100 gas flaring impact was observed at the Tiksi station (northeastern Siberia), despite the large
101 distance of the station from the largest oil and gas producing regions (Winiger et al., 2017). To
102 better understand and quantify the contribution of gas flaring to the Arctic environment, targeted
103 aerosol and atmospheric composition measurements at the closest distance from the flaring
104 facilities are needed. The present operating Eurasian Arctic stations are all too far away to allow
105 assessing how air masses are affected by gas flares or what the contribution from different source
106 categories is (Stohl et al., 2013). Simulations combined with observations of BC at the proximity
107 of the source regions (e.g., the plumes from gas flaring regions over the Kara Sea) provide a better
108 constraint (Popovicheva et al., 2017). In addition, measurements of BC coupled by conditional
109 probability simulations performed inside the oil and gas producing region of the northwestern
110 Siberia have successfully distinguished between multiple industrial and urban sources
111 (Popovicheva et al., 2020).

112 Recent efforts have sought to develop a new Russian BC emission inventory (BCRUS) for
113 the Siberian Arctic, based on activity data from local information, improved spatial distribution of
114 BC emissions and updated emission factors for oil and gas fields in northwestern Siberia (Huang
115 et al., 2015). According to this, it was found that BC emissions from gas flaring account for 36%
116 of the total anthropogenic BC emissions over Russia. Residential BC emissions, transportation,
117 industry, and power plants contribute 25%, 20%, 13%, and 5.4%, respectively. The emissions from
118 gas flaring in BCRUS show a discrepancy of more than 40% higher than ECLIPSEv5. Using
119 BCRUS, modelled surface BC at Zeppelin, Barrow, and Alert stations were basically improved
120 (Huang et al., 2015). The contribution of anthropogenic emissions in Russia to the annual total
121 Arctic surface BC were calculated to be 56%, with gas flaring from the Yamalo-Nenets
122 Autonomous Okrug (YNAO), Khanty-Mansiysk Autonomous Okrug (KMAO), and Komi
123 Republic to be the main source (31% of Arctic surface BC) (Zhu et al., 2020). However, due to
124 the absence of BC inventories for industrial emissions and a denser observational network in the
125 western Siberian High Arctic, the spatial distribution of BC sources is still associated with large
126 uncertainties.

127 Agricultural fires in East Europe and North America are a major source of biomass burning
128 in the Eurasian Arctic (Treffeisen et al., 2007; Stohl et al., 2007; Stohl et al., 2006). Springtime
129 fires in Siberia can double the North American Arctic background (Warneke et al., 2010). Long-
130 term airborne observations of BC in Northern Siberia have revealed a strong impact from forest
131 fires in summer (Kozlov et al., 2016; Paris et al., 2009). Particulate BrC emitted by intensive
132 wildfires has been measured in plumes transported for over two days (Forrister et al., 2015). In
133 summer 2019, wildfire activity in Central and Eastern Siberia occurred along the trans-Arctic
134 transport pathway of Siberian biomass burning emissions resulting in enhanced aerosol lamina
135 observed in Western Canada (Johnson et al., 2021).

136 In 2019, a new aerosol station was developed by Moscow State University on the Bely Island
137 located in the Kara Sea (Western Siberian Arctic) ([https://peexhq.home.blog/2019/12/11/new-
138 research-aerosol-stations-in-the-russian-arctic](https://peexhq.home.blog/2019/12/11/new-research-aerosol-stations-in-the-russian-arctic)), (Figure 1). The region was chosen because it is
139 close to the air pathway of large-scale emission plumes from populated industrial regions of
140 Eurasia and Siberian wildfires to the Arctic. We present here the ground-based continuous BC
141 (equivalent BC, EBC) measurements from August 2019 until November 2020 at the “Island Bely”
142 station for the first time. The Arctic annual trends of BC are assessed, while the geospatial source
143 origin of the air arriving at the station is identified using a Lagrangian particle dispersion model.
144 Furthermore, the anthropogenic and biomass burning contributions to the modelled surface
145 concentrations of BC are evaluated against measured BC concentrations at the station.

146 Characterization of the pollution events in cold and warm periods separates the impact of gas
147 flaring versus biomass burning. In addition, the spectrally resolved absorption measurements
148 provide an opportunity for the characterization of BC sources. The present study assesses long
149 range transport of BC to the Western Siberian Arctic from the main large-scale emission regions
150 of the Eurasian continent using Lagrangian modelling coupled with continuous observations.

151 **2 Experimental**

152 **2.1 Aerosol station “Island Bely”.**

153 Western Siberia is the world's largest gas flaring region with a leading oil and gas production
154 industry (**Figure 1**). YNAO is located north of the West Siberian Plain and covers a vast area of
155 769 thousand km². More than 94% of the region's economy is associated with industrial
156 applications related to the extraction of fuels, their processing, and transportation. Specifically,
157 YNAO has the largest reserves of Russia's natural gas and oil; YNAO emissions of BC are the
158 largest in the Russian territory (Vinogradova, 2015). The relative contributions from gas flaring to
159 annual mean BC surface concentrations from all emission sources (surface transportation,
160 industry, residential, biomass burning) exceed 70% (Stohl et al., 2013).

161 The Bely Island is located in the Kara Sea, north of the YNAO (**Figure 1**). For the purpose
162 of atmospheric composition observations and sampling at the “Island Bely” station, the aerosol
163 pavilion has been built approximately half a km to the southeast of the Roshydromet
164 meteorological station continuously operating at the island (**Figure 1**). There are no other
165 anthropogenic constructions on the island. Thus, the major advantage of a new-developed research
166 station is its long distance from any local anthropogenic sources. Previous research at the Tiksi
167 station has shown significant aerosol pollution from local sources (Popovicheva et al., 2019),
168 which is not the case in the “Island Bely” station. An aerosol sampling system was installed at the
169 aerosol pavilion in May 2019. Three total suspended particle (TSP) inlets were installed
170 approximately 1.5 m above the roof and 4 m above the ground. One is used for the real-time BC
171 monitoring with air flow 5 L/min, and two for aerosol chemical characterization operating with
172 2.3 m³/h flow. The TSP inlet is equipped with an electric heating wire to prevent rimming and ice
173 blocking of the system.

174 An Aethalometer model AE33 (Magee Scientific, Aerosol d.o.o.) was used to measure the
175 light attenuation caused by particles depositing on two filter spots at different flow rates (Drinovec
176 et al., 2015) and at seven wavelengths from ultraviolet (370 nm) to infrared (950 nm). The “dual
177 spot” technique is applied for real-time loading effect compensation. The light-absorbing content
178 of carbonaceous aerosol at 880 nm is reported as equivalent black carbon concentration (EBC),

179 which is determined for each time interval from the change in the light attenuation at a wavelength
180 of 880, using a mass absorption cross-section of 7.7 m²/g and filter multiple scattering parameter
181 C of 1.57. Light absorbing organic components (BrC) absorb light at shorter wavelengths more
182 effectively than at 880 nm, which is observed as an increased AAE (Sandradewi et al., 2008;
183 Grange et al., 2020; Helin et al., 2021). AAE was calculated using Eq. 1 for 470 nm and 950 nm
184 wavelengths:

$$185 \quad AAE = \frac{\ln(b_{abs}(470)/b_{abs}(950))}{\ln(950/470)} \quad (1)$$

186 where b_{abs} stands for the absorption coefficient at 470 nm and 950 nm. In order to avoid
187 instrumental noise when calculating the AAE, the following data processing was implemented.
188 One-minute absorption coefficients for the whole period were averaged to 1 hour. The dataset was
189 filtered to periods when EBC exceeded 20 ng/m³ (sensitivity level at 1 hour time resolution), and
190 then the AAE was averaged to 3 hours.

191 The Aethalometer model (Sandradewi et al., 2008) is typically used for the source
192 apportionment of EBC, when measurements of absorption coefficient are performed by filter
193 photometers. The model uses an a priori assumed pair of AAE for traffic (AAETR) and biomass
194 burning (AAEBB) to determine the contribution of both sources. Although the Aethalometer
195 model is an efficient tool for source apportionment of EBC in a well-mixed urban atmosphere,
196 where two sources with distinct aerosol optical properties prevail (fossil fuel from traffic and fresh
197 biomass burning), the results can be affected when the characteristic optical properties of a specific
198 source change over time. This is usually the case for wildfires, where different burning modes
199 (flaming or smoldering) and different types of wood can significantly influence BrC emissions and
200 its chemical composition (Kalogridis et al., 2018b). Furthermore, chemical evolution after
201 emissions and atmospheric aging (i.e. aerosol mixing state, particle morphology and size
202 distribution) additionally influence aerosol absorption, which can be noticed especially for long-
203 range transported air masses (Cappa et al., 2016; Saleh et al., 2013; Romshoo et al., 2021).
204 (Forrister et al., 2015) have shown that BrC emitted from wildfires was highly unstable, with 6%
205 of BrC remaining above background levels after two days.

206 BC measurements at the “Island Bely” station were performed from 10 August 2019 to 30
207 November 2020, with a time resolution of 1 min. Basic meteorological parameters, such as
208 temperature, wind speed and direction were obtained every 3 hours from a meteorological station
209 located 500 m from the “Island Bely” station. Cleaning of 1-min time resolved BC data was based
210 on the definition of what can be considered as a peak: strong fast increase of BC value a few times
211 higher than previous value and then a similar fast decrease. Analysis of meteorological parameters

212 was complementary to check whether the wind originated from the sector corresponding to
213 locations of diesel generators at the Roshydromet meteorological station (240-250 degrees from
214 the “Bely Island” station). In such cases, strong peaks of BC were removed from further analysis.
215 The total duration of the peaks under the influence of local contamination varies from several
216 minutes to one–two hours per day and monthly. For instance, in January 2020, when wind blew
217 from 240-250 degrees for 24 hours in total, large peaks corresponding to a fraction of 13% of the
218 data were removed. In July 2020, when wind originated from the same location for a total of 45
219 hours, measurements corresponding to a fraction of 22% of the data were removed. Lack of windy
220 weather at Bely Island is a very rare event, only 0.7% of the observation time; during such weather,
221 peaks of BC were never observed.

222 **2.2 Atmospheric transport model coupling with emissions**

223 To investigate the possible origin of BC, the Lagrangian particle dispersion model
224 FLEXPART (FLEXible PARTicle dispersion model) version 10.4 was used (Pisso et al., 2019).
225 The model was driven by 3-h operational meteorological fields from the European Centre for
226 Medium-Range Weather Forecasts (ECMWF) with 137 vertical levels and a horizontal resolution
227 of $1^\circ \times 1^\circ$. In FLEXPART, computational particles were released at height 0 - 100 m from the
228 receptor (“Island Bely” station) and were tracked backward in time in FLEXPART’s “retroplume”
229 mode. Simulations extended over 30 days backward in time, sufficient to include most BC
230 emissions arriving at the station, given a typical BC lifetime of 1 week (Bond et al., 2013).

231 The tracking includes gravitational settling for spherical particles of the size observed.
232 FLEXPART differs from trajectory models due to its ability to simulate dry and wet deposition of
233 gases or aerosols (Grythe et al., 2017), turbulence (Cassiani et al., 2015), unresolved mesoscale
234 motions (Stohl et al., 2005), while it includes a deep convection scheme (Forster et al., 2007). For
235 our simulations, we assumed that BC has a density of 1500 kg m^{-3} and follows a logarithmic size
236 distribution with an aerodynamic mean diameter of $0.25 \text{ }\mu\text{m}$ and a logarithmic standard deviation
237 of 0.3 (Long et al., 2013).

238 FLEXPART simulations were performed every 3 hours during the studied period. The
239 FLEXPART output consists of a footprint emission sensitivity which results in a modelled
240 concentration at the receptor, when coupled with gridded emissions from an emission inventory.
241 The emission sensitivity expresses the probability of any release occurring in each grid-cell to
242 reach the receptor. The source contributions to receptor BC were derived by combining each
243 gridded emission sector (e.g. gas flaring, transportation, waste management etc...) from an
244 emission inventory with the footprint emission sensitivity. Calculations for anthropogenic sources

245 (emission sectors are described below) and open biomass burning were performed separately. This
246 enabled identification of the exact origin of BC and allowed for quantification of its source
247 contribution. The modelled concentrations can also be displayed as a function of the time elapsed
248 since the emission has occurred (i.e., "age"), which can be shown as "age spectrum".

249 In this study, anthropogenic emission fluxes were adopted from the latest version (v6b) of
250 the ECLIPSE (Evaluating the CLimate and Air Quality ImPacts of Shortlived Pollutants) dataset,
251 an upgraded version of the previous version (Klimont et al., 2017). The inventory includes
252 industrial combustion (IND) emissions from industrial boilers and industrial production processes.
253 Energy production sector (ENE) includes emissions from combustion processes in power plants
254 and generators. Residential and commercial sector (DOM) includes emissions from combustion in
255 heating and cooking stoves and boilers in households and public and commercial buildings. Waste
256 treatment and disposal sector (WST) resembles emissions from waste incineration and treatment.
257 Transport sector (TRA) includes emissions from all land-based transport of goods, animals and
258 persons on road networks and off-road activities. Emissions from shipping activities in in-land
259 waters (SHP) is included as a separate sector. Gas flaring (FLR) sector includes emissions from
260 oil and gas facilities. The methodology for obtaining emissions from FLR specifically over Russia
261 has been improved in ECLIPSEv6 (Böttcher et al., 2021). Updates were based on new field-type
262 specific emission factors that were applied to VIIRS observations of the flared gas volume at
263 individual flaring locations. For comparison, BCRUS emissions for the FLR sector (Huang et al.,
264 2015) were also used in this study.

265 Emissions from biomass burning (BB) were adopted from Copernicus Atmosphere
266 Monitoring Services (CAMS) Global Fire Assimilation System (GFAS). CAMS GFAS assimilates
267 fire radiative power (FRP) observations from satellite-based sensors converting the energy
268 released during fire combustion into gases and aerosol daily fluxes (Di Giuseppe et al., 2016;
269 Kaiser et al., 2012). Data are available globally on a regular grid with a horizontal resolution of
270 0.1 degrees from 2003 to the present. FRP observations assimilated in GFAS are the NASA Terra
271 MODIS and Aqua MODIS active fire products (<http://modis-fire.umd.edu/>, (Kaufman et al.,
272 2003). FRP measures the heat power emitted by fires, as a result of the combustion process and is
273 directly related to the total biomass combusted (Wooster et al., 2005). Using land-use-dependent
274 conversion factors, GFAS converts FRP into emission estimates for 44 smoke constituents (Kaiser
275 et al., 2012), one of which is BC.

276 Biomass burning emissions were also adopted from the Global Fire Emission Dataset
277 version 4.1 (GFEDv4.1). The product combines satellite information on fire activity and
278 vegetation productivity to estimate gridded monthly burned area and fire emissions, as well as

279 scalars that can be used to calculate higher temporal resolution emissions. All data are publicly
280 available for use in large-scale atmospheric and biogeochemical studies and include (i) burned
281 area (Giglio et al., 2013) , (ii) burned area from "small" fires based on active fire detections outside
282 the burned area maps detailed in (Randerson et al., 2012) and updates in (Werf et al., 2017), (iii)
283 carbon and dry matter emissions from van der Werf et al. (2017), (iv) fractional contributions of
284 various fire types to total emissions and (v) list of emission factors to compute trace gas and aerosol
285 emissions based on (Akagi et al., 2011) and (Andreae and Merlet, 2001). The current version (v4)
286 has a spatial resolution of 0.25 degrees and is available from 1997 onwards.

287 In the present paper, several different configurations were used to calculate modelled
288 surface BC concentrations at "Island Bely" station, namely ECLIPSEv6 with GFED4
289 (ECLIPSEv6-GFED4), and ECLIPSEv6 with CAMS (ECLIPSEv6-CAMS). The same two
290 configurations were also used after substituting the FLR emissions in ECLIPSEv6 with those from
291 BCRUS (Huang et al., 2015).

292 **3 Results and discussion**

293 **3.1 Monthly climatology of black carbon**

294 The climate at the Bely Island is characterized by an average annual temperature of -8°C,
295 precipitation of 450 mm, and stable snow coverage from October to May. Meteorology displays a
296 large annual variability determined by alternating periods of the polar night and midnight sun.
297 Median temperatures stay above 0°C for 4 months each year between June and September. This
298 period is also characterized by the highest-frequency occurrence of ocean air masses and the most
299 stable wind speeds. A shift occurred in October with decreased solar insolation resulting in a
300 temperature shift to below 0°C. The cold month winds were primarily continental, with a low-
301 frequency occurrence of ocean air masses.

302 The cycle of temperature and wind speed variations observed during the study period is
303 shown in **Figure 2a,b**. The period from 1 November 2019 to 1 April 2020, when temperature
304 dropped below -10 °C, as well as November 2020, is denoted as the "cold period". The remaining
305 period of our study, from 10 August to 31 October 2019 as well as from April to 1 November
306 2020, is considered as the "warm period". **Figure 2c** illustrates the long-term time series of 24h
307 median EBC concentrations measured at wavelength of 880 nm (EBC(880)) during the study
308 period, with median value $37 \pm 64 \text{ ng/m}^3$ (maximum: 520 ng/m^3 , minimum: 6 ng/m^3). The polar
309 frequency plot of wind speed/direction shows that the maximum number of hours the wind was
310 from north-east and south-west directions with around 5 m/s (**Figure 3a**). BC concentration rises

311 in **Figure 3** indicate the sources of the highest concentrations, which originated from the continent
312 in both cold and warm periods.

313 **Figure 4** illustrates a long-term time series of monthly EBC concentrations at the “Island
314 Bely” station during the period from August 2019 to November 2020. The highest concentrations
315 were observed from November to April and the lowest ones from June to August, in agreement
316 with the typical seasonal trend of the Arctic aerosol concentrations (Stone et al., 2014). EBC
317 monthly climatology during the study period is shown in **Figure 4a** in terms of the median, and
318 upper and lower quartiles. For winter months, the maximum median EBC concentration was 165
319 ng/m^3 observed in December 2019. The increase of the Arctic concentrations in winter, known as
320 the Arctic Haze, was more pronounced in November-December 2019 and January-March 2020.
321 On average, concentrations in summer were about 10 times lower than those in winter, with a
322 minimum median value of $30 \text{ ng}/\text{m}^3$ in July 2020. Observations at the “Island Bely” station for the
323 second year started from August 2020 and lasted to November 2020 to confirm the general annual
324 trend of low summer and high winter BC concentrations. However, monthly median EBC in
325 September 2020 demonstrated a value of $30.7 \text{ ng}/\text{m}^3$.

326 Similar annual trend was recorded in 2015-2016 at the Tiksi station (coast of Laptev sea),
327 with high concentrations reaching $130 \text{ ng}/\text{m}^3$ during winter-spring and low concentrations of about
328 $20 \text{ ng}/\text{m}^3$ observed from May to October (Popovicheva et al., 2019b). As shown by earlier studies
329 at various polar stations, such as in Ny-Ålesund, Alert, and Barrow, aerosols display Arctic Haze
330 peak concentrations during winter and early spring months (Stone et al., 2014). EBC during Arctic
331 Haze at both “Island Bely” and Tiksi stations are typically higher as compared to those observed
332 at Alert ($100 \pm 65 \text{ ng}/\text{m}^3$), a station that has shown the largest concentrations among all Polar
333 stations (Sharma et al., 2004). The latter confirms previous findings from (Eckhardt et al., 2015)
334 and (Winiger et al., 2017) that the Siberian Arctic is mainly polluted as a result of the influence
335 from emissions occurring in the Eurasian continent.

336 Near-surface measurements allow for evaluation of the capability of transport models to
337 reproduce the distribution of BC in the Arctic based on different emission datasets (Schacht et al.,
338 2019; Zhu et al., 2020). **Figure 4a** and Supplementary Table S 2 show observed and modelled BC
339 monthly median mass concentrations at the “Island Bely” station. Use of ECLIPSEv6 emissions
340 caused overestimations of modelled BC concentrations of up to 46% (February 2020). All
341 simulated BC concentrations were found in the range between the 25th and 75th percentiles of
342 measured EBC. Modelled BC is underestimated in March-May 2020, being $29 \text{ ng}/\text{m}^3$ below the
343 25th percentile of EBC in April 2020. When FLR emissions in ECLIPSEv6 were substituted by
344 BCRUS FLR, similar modelled BC monthly median concentrations were calculated, thus

345 indicating that other sectorial emissions might have a large contribution to surface BC at the
346 station.

347 **Figure 4b** shows the so-called “age spectrum” of modelled BC for the “Island Bely”
348 station. In the cold period of high EBC concentrations, the longest age of more than 19 days back,
349 affects up to 60% of the surface concentrations. In this time, due to the geographical proximity,
350 Russia dominates. However, both Europe and Asia contribute around 20% to the monthly averaged
351 surface BC, with the largest contribution to be in February 2019 and November 2020, (**Figure**
352 **4b,d**). The most aged air masses (from 28 to 30 days back) contributed up to 50%, arriving at the
353 “Island Bely” station in December 2019, which is the month of the highest observed EBC
354 concentrations during the study period. The impact of the closest regions with age between 7 and
355 9 days is more significant in the winter months, while in the warm period, such short-term
356 contributions become negligible. The calculated age and continental spectrum of BC obtained for
357 the “Island Bely” station mainly denote the variability of airmass transport patterns in different
358 seasons. In the cold season, the Siberian Arctic tends to force the air from south to north into the
359 Arctic (Stohl, 2006), thus bringing more anthropogenic BC from highly populated regions.

360 Monthly averaged BC contributions from different sources simulated by FLEXPART
361 using ECLIPSEv6 emissions are shown in **Figure 4c** and Supplementary Table S 3. From
362 November 2019 to March 2020 the FLR sector contributed 47%–68% (maximum in January 2020)
363 to surface BC, when air masses arrived at Bely through oil and gas extraction sites. February and
364 November 2020 demonstrated the biggest non-gas flaring impact. More specifically, February
365 2020 coincides with the largest model overestimation (**Figure 4a**) implying a likely misestimation
366 of non-gas flaring emissions in ECLIPSEv6. From April 2020 the impact of FLR dropped
367 significantly (Supplementary Table S 4), with minimum of 12% in June. Starting from April to
368 October 2020, BB emissions played the biggest role in surface BC contributing 81% in July 2020.
369 It is noteworthy that the impact of SHP emissions became quite perceptible in the warm period,
370 when the oceanic ice is absent in the Arctic and touristic cruises peak.

371 Emission sensitivities of surface BC presented over the whole Arctic (north of 66°N) have
372 been also simulated using the same model (Zhu et al., 2020). Anthropogenic sources contributed
373 82% of the annual BC, as estimated from BCRUS emission dataset. Arctic BC originated
374 predominantly from anthropogenic emissions in Russia (56%), mainly FLR from YNAO, Khanty-
375 Mansiysk Autonomous Okrug (KMAO), and Komi Republic (31% of surface Arctic BC). In
376 summer (July-August), open BB in Siberia, Alaska, and Canada contributed 75%. At Zeppelin,
377 modelled BC (39.1 ng/m^3 for annual mean) was reported to be 85% higher than the observed value
378 (21.1 ng/m^3 for annual mean) (Zhu et al., 2020). At Tiksi, modelled BC was underestimated (74.4

379 ng/m³ for annual mean) by 40% compared with observations (104.2 ng/m³ for annual mean) (Zhu
380 et al., 2020). Annual (from September 2019 to August 2020) median modelled concentrations of
381 BC using ECLIPSEv6, BCRUS, and CAMS for the “Island Bely” station are shown in
382 Supplementary Table S 2. We find that modelled BC (78.4 ng/m³ for annual mean) is 26% higher
383 than the observed value (61.8 ng/m³ for annual mean); the overestimation is much smaller than
384 observed for other remote stations. Annual averaged contributions of anthropogenic emissions by
385 ECLIPSEv6 and ECLIPSEv6 with flaring from BCRUS were equal to 76% and 80%, respectively,
386 due to the difference in FLR emissions in the two datasets (Supplementary Table S 4).

387 **3.2 Cold season pollution**

388 **Figure 5a** shows EBC concentrations measured at the “Island Bely” station during the cold
389 period, from November 2019 to April 2020 and from 1st to 30th November 2020. Time series
390 indicates that EBC undergoes the Arctic-typical seasonal trend with higher concentrations in
391 winter and early spring and lower in summer. Background pollutant concentrations in Arctic
392 stations are generally very low without any detectable influence from local or regional sources
393 (Eleftheriadis et al., 2004; Popovicheva et al., 2019b). We relate the Arctic background to the
394 lowest 20th percentile of EBC data (10 ng/m³). Long-term pollution episodes were assumed to be
395 repeated events of high EBC concentration above the 80th percentiles (90 ng/m³) that are clearly
396 distinguishable from the background (**Figure 5a**).

397 The aerosol optical properties with respect to absorption, presented as daily median AAE
398 is shown in **Figure 2d**. The AAE for highly aged aerosols measured during periods of low BC was
399 lower than 1 (reaching values as low as 0.2) and is mostly related to the aerosol size distribution
400 (large particles) and internally mixed BC particles (Cappa et al., 2016). As shown by modeling
401 studies (Virkkula, 2021), pure BC particles surrounded by non-absorbing coatings can have AAE
402 in the range from <1 to 1.7, also depending on the morphology of the fractal aggregates (Romshoo
403 et al., 2021). The AAE increased in periods of higher aerosol concentration levels in the cold
404 period ranging from 0.6 to 1.35.

405 In many cases, when AAE exceeded 1 in the cold period, the pollution episodes could be
406 identified as influenced by BB. However, due to the mixing with background aerosol and aging
407 processes, a large variability in AAE values might be observed at receptors of long range
408 transported pollution and AAE may not be representative of BB sources. Nevertheless, it can still
409 be used as a qualitative parameter, when extra information is available. Such events of increased
410 AAE were rarely observed in our study, and the most prominent BB impact occurred during the
411 pollution episodes C4, C7, and C8 when impact of domestic sources was significant (**Figure 5a**).

412 In general, FLEXPART coupled with ECLIPSEv6-CAMS emissions captures periods with
413 both high and low concentrations relatively well, (**Figure 2c**). A good correlation between
414 measurements and simulations, with a Pearson coefficient R of 0.7 and the root mean squared error
415 (RMSE) of 89.2 ng/m³ was obtained for the cold period (**Figure 6a**). According to monthly median
416 contributions to BC concentrations in the cold period, the impact of anthropogenic sources, namely
417 FLR, DOM and TRA dominated surface BC by 97.7% (**Figure 4c**).

418 Looking closely to specific episodes, during pollution episode C1, three events of high
419 EBC concentrations were observed, (**Figure 5a**). On 5 November 2019, measured EBC reached
420 180 ng/m³, while FLEXPART simulated similarly high BC values. Footprint emission sensitivities
421 at this time showed that airmasses originated from East and North Europe, passed south of
422 European Russia, then turned the direction straight through the West Siberia approaching the Bely
423 Island from the southeast (**Figure 7**). The same airmass moved towards the large Russian FLR
424 sources of YNAO, KMAO, and Krasnoyarsky Krai (see **Figure 1**) causing up to 71% contribution
425 to surface BC (Supplementary Table S 5).

426 On 12 November 2019, airmasses arrived at the Bely Island through the Yamal peninsula
427 after passing from the ocean (Supplementary Figure S 1). Model strongly underestimated
428 measured EBC concentrations by about 10 times (**Figure 7**). We fail to provide a concrete
429 explanation for this; a simplified hypothesis is that a number of flaring sites located at the Yamal
430 peninsula might have not been included into the emission database, but this certainly needs further
431 research. In contrast, the model strongly overestimated measured EBC concentrations on 16
432 November 2019. At that time, airmasses passed through remote regions of Eastern Siberia and
433 arrived through the gas flaring sites of Krasnoyarsky Krai at the station (**Figure 7**) causing an FLR
434 contribution of 98.6% to surface BC (Supplementary Table S 5). The reason might be use of
435 incorrect emission factors for BC at the FLR facilities of Krasnoyarsky Krai in the adopted
436 emissions, because direct transport from this region was observed. During 12 and 16 November
437 2019 the AAE was in the range from 0.7 to 1, which agrees with the expected optical properties
438 for the FLR sources.

439 Pollution episode C2 in December 2019 gave the highest EBC concentrations observed
440 during the whole cold period, (**Figure 5a**). On 4 December, EBC approached 400 ng/m³, when
441 airmasses originated from Kazakhstan and Russian gas flaring regions of KMAO and YNAO
442 (**Figure 8**). The maximum EBC concentration of approximately 500 ng/m³ with AAE 1.05 was
443 observed on 19 December, when air came from Europe, initially through the Russian oil and gas
444 basins of Volga-Ural at the south of European Russia and then through KMAO and YNAO in

445 Western Siberia (**Figure 8**). During the December pollution events, FLR contribution dominated,
446 reaching 73% on 19 December (Supplementary Table S 5).

447 The highest FLR contributions were observed during the pollution episodes C3–C6
448 (Supplementary Table S 5). Similar air mass transportation through either gas and oil fields of
449 YNAO and KMAO in Western Siberia or Komi and Nenets regions north of European Russia
450 occurred in all of the events, (Supplementary Figure S 1).

451 In contrast to the aforementioned events, the pollution episode C7 was unrelated to FLR,
452 as air masses did not cross flaring regions (**Figure 8**). On 16 November 2020, retroplumes confirm
453 origin of surface BC from Central and Eastern Europe and the Kola Peninsula (**Figure 8**). DOM
454 and TRA hold the largest share of the source contribution with 73% and 20%, respectively
455 (Supplementary Table S 5), while the model overestimated measured EBC. Episode C8 gave the
456 biggest EBC (370) concentration which reached 346 ng/m³ and exceeded EBC (880) (133 ng/m³)
457 on 24 November 2020 (Supplementary Table S 5). At this time, air masses came to the Bely Island
458 directly from the most populated region of European Russia (**Figure 8**). The contribution of DOM
459 and TRA was 34% and 23%, respectively. AAE approached the highest value observed (1.3)
460 during the study period. This might show a detectable impact of biomass burning in the classified
461 DOM emissions. BC from wood burning contributes around 61% of the total residential emissions,
462 especially in areas where there is limited use of natural gas (Kalogridis et al., 2018a), and in forest
463 regions (Huang et al., 2015). Note that the impact of IND emissions was the largest in episodes
464 C7 and C8 as compared to the whole cold period (Supplementary Table S 5), due to industrial
465 emissions from sites in Central European Russia.

466 **3.3 Warm season pollution**

467 **Figure 5b** shows EBC concentrations measured at the “Island Bely” station during the
468 warm period, from 10 August to 31 October 2019 and from 1 April to 1 November 2020. It is
469 immediately seen that BC in the warm period was mainly affected by Russian emissions (90%),
470 and only in October 2020 and August 2019 partly (~20%) from Europe and North America,
471 (**Figure 4**). EBC concentrations rarely exceeded the 80th percentile that was set as the pollution
472 criterion, while the duration of the warm period episodes was shorter.

473 Due to the mixing with background aerosol and aging processes, air masses influenced by
474 BB events should be expected to have increased AAE as compared to the BC produced by fossil
475 fuel. However, aging processes may induce a high variability in AAE in areas affected by long-
476 range transport, and hence AAE may not be representative of a BB source. Pollution events were

477 rarely observed in this season, and the most sufficient BB impact occurred during the pollution
478 episodes W4, W7, and W8.

479 However, events characterised by higher AAE were observed more often indicating that
480 BB impact was more significant during the warm period, mainly during spring and summer
481 (episodes W3, W4, and W6). Comparison between measured and modelled concentrations showed
482 poor correlation (R of 0.41 and RMSE of 121 ng/m³) (**Figure 6**). According to monthly median
483 contributions to surface BC concentrations in the warm period, the impact of BB emissions was
484 as high as 50% (**Figure 4c**). SHP emissions contributed about 1%, as a result of the increase of
485 touristic activity in the Arctic and the more active use of the Northern Sea Route due to the Arctic
486 ice retreat.

487 From the beginning of the study period in August 2019, large wildfires were observed in
488 Siberia (Voronova et al., 2020). The latter resulted in a strong BB impact at the “Island Bely”
489 station (**Figure 5b**). However, during episode W1, EBC concentrations reached approximately 200
490 ng/m³ not caused by wildfire plumes (**Figure 5**). During this time, airmasses were transported
491 from Northern Europe (Supplementary Figure S 1), and the main contribution to surface BC at the
492 “Island Bely” station was due to TRA emissions (36%, Supplementary Table S 5).

493 Episode W2 during October 2019 (**Figure 5**) was characterised by EBC of 119 ng/m³,
494 while modelled BC was strongly overestimated (Supplementary Figure S 1). The calculated BB
495 contribution to station’s surface BC was 64% (Supplementary Table S 5) and the hotspot BB
496 sources were near the Pur River (YNAO), as recorded by CAMS (Supplementary Figure S 1). The
497 measured AAE does not indicate any contribution from BrC, as it would be expected for BB
498 sources and observed AAE values were lower than 1 (Supplementary Table S 5). Note that the
499 FIRMS active fire data analyses (<https://firms.modaps.eosdis.nasa.gov/>) indicate that the fire spots
500 were in the same grid-cell as industrial facilities of oil extraction field in the Purovski region
501 (YNAO). Thus, it might be that thermal anomalies from flaring facilities were mistakenly related
502 to fires in CAMS. This hypothesis is reinforced by the fact that no wildfires were recorded by the
503 local forest fire service (<https://aviales.ru>) during October 2020 in Western Siberia and
504 Krasnoyarsky Krai.

505 Pollution episode W3 is related to a strong springtime wildfire activity that occurred in
506 Southern Siberia. The retroplumes on 18 and 23 April 2020 showed that the air originated from
507 Central Asia, a large territory of Southern Siberia and Krasnoyarsk Kray, and arrived at the Bely
508 Island through the Western Siberia from the southeast (Supplementary Figure S 1, **Figure 9**). High
509 footprint emission sensitivities coincided with the location of large wildfires resulting in BB

510 contribution to surface BC at the station equal to 28% (18 April 2020) and 19% (23 April 2020),
511 respectively. The most significant impact of wildfires was observed on 23 April 2020, when 6-h
512 median EBC concentration reached 700 ng/m³ with AAE ranging from 1.3 to 1.5, clearly
513 indicating an elevated contribution of BrC (Supplementary Table S 5).

514 Wildfires occurred in northern Krasnoyarsk Krai and Sakha Republic, Central Siberia
515 between April and November 2020 (<https://aviales.ru/popup.aspx?news=6286>) that burned around
516 seven million hectares of forest. The pollution episode W4 on 7 July 2020 recorded a 6-h median
517 EBC of 150 ng/m³ and an AAE of around 1.4 clearly indicating BB impact. The model captures
518 this event well, providing the highest BB contribution exactly when observed, equal to 90%
519 (Supplementary Table S 5). Airmasses arrived from the east and passed north of Krasnoyarsk Kray
520 where the large wildfires occurred (**Figure 9**).

521 Unprecedented high wildfire-related BC concentration was observed in September 2020
522 (pollution episode W6). EBC concentrations exceeded 5 and 20 times the 80th percentile of the
523 measurements. Maximum 6-h median EBC reached 534 ng/m³ on 1st September 2020 and it was
524 even higher than the biggest Arctic haze concentration observed in December 2019,
525 (Supplementary Table S 5). Increased AAE of around 1.4 revealed strong BB impact. This event
526 resulted from long-range transport of BC from the Eurasian continent during the intensive
527 wildfires in Western Siberia (Krasnoyarsk Kray and Yakutia) (**Figure 9**), where around one
528 million hectares of forest were burned in August 2020. The contribution of BB to surface BC at
529 the “Island Bely” station was as high as 95%.

530 Despite the exclusive BB origin of the light absorbing carbon measured at the “Island Bely”
531 station, the AAE was much lower than the established value for fresh BB (close to 2) (Sandradewi
532 et al., 2008) likely due to aging. This apparent reduction of the BrC contribution to absorption is
533 in agreement with (Forrister et al., 2015), who examined BrC concentrations and AAE from
534 Western U.S. forest fires as a function of aging. Their results show that most of the BrC (~94%)
535 emitted from wildfires was lost within a day. Similar observations have been reported for long-
536 range transported North American smoke over the Northeastern Atlantic (Zheng et al., 2020) and
537 for transported Russian smoke over the Mediterranean (Diapouli et al., 2014).

538 The last pollution episode W7 was observed at the end of October 2020. Although it
539 occurred in the warm period, it is rather related to Russian FLR and European TRA emissions
540 (Supplementary Table S 5, **Figure 5b**). At the end of October 2020 airmasses came mainly from
541 Europe, passing through the Yamal Peninsula.

542 **4 Conclusions**

543 The present paper aims at performing a quantitative analysis of the Arctic pollution via
544 high-resolution measurements from a recently developed aerosol station at the Bely Island (Kara
545 Sea) combined with Lagrangian modelling. A consequent goal is to examine the impact of
546 anthropogenic and natural sources to the high Arctic as a result of long-range transport. The main
547 results can be summarised as follows:

- 548 - EBC monthly climatology is following the typical Arctic aerosol seasonal variation
549 characterised with higher EBC concentrations in winter and lower in summer.
- 550 - AAE for aged BC larger than 1 indicates wildfire impact in the warm period, but mixing with
551 gas flaring emissions from nearby regions was also observed.
- 552 - The recently upgraded ECLIPSEv6 emissions and ECLIPSEv6 coupled with FLR from
553 BCRUS represent measured EBC accurately in the cold period. Annual average contributions
554 of anthropogenic emissions to surface BC were 76% and 80% (50% and 59% from gas flaring)
555 for each dataset, respectively.
- 556 - The most significant model overestimation was observed in February 2020, when air masses
557 passed through non gas flaring regions. The largest underestimation occurred in April 2020
558 during the period of spring agriculture fires.
- 559 - Daily BB emissions from CAMS were more efficient in representing pollution episodes than
560 monthly GFED4 emissions, and therefore they were mainly used here.
- 561 - Russian emissions dominate during the whole year, European and Asian ones contribute up
562 to 20% in the cold period. Pollution episodes with EBC concentrations above 90 ng/m^3 occur
563 in 18.5% of observation time. Monthly average FLR emissions dominate (98%) any other
564 emission sector.
- 565 - FLR and BB emissions contribute the largest share of EBC to the “Island Bely” station during
566 the cold and warm period, respectively. This is consistent with previously-reported source
567 contributions to the the Russian Arctic. When air is transported from Europe, other sources
568 such as TRA become important. The same applies for SHP emissions that become important
569 in summertime, because of cruise activities and ice retreat.
- 570 - Emissions from gas and oil fields in Western Siberia, and the Northern European Russia cause
571 the vast majority of the pollution episodes in the Arctic.
- 572 - 15 pollution episodes with concentrations reaching close to 723 ng/m^3 were detected. The
573 duration of the cold pollution episodes is longer than of the warm period, and the median (up
574 to 160 ng/m^3) and maximum EBC (up to 450 ng/m^3) concentrations higher.

575 In conclusion, the significance of high-quality measurements at the “Island Bely” station
576 is pronounced from the present study, because (i) the station is located along the main pathway of

577 airmasses entering the Arctic, and (ii) it is north of the world's largest gas flaring regions. The
578 operation of the "Island Bely" station is an asset in source emission optimisation, because EBC
579 measurements in the High Arctic are still rare.

580

581 *Data availability.* All model data used in the present publication together with all figures of
582 footprint analysis and source contributions to surface BC are open through the websites
583 https://niflheim.nilu.no/NikolaosPY/Bely_2020_cams.py and
584 https://niflheim.nilu.no/NikolaosPY/Bely_2020_huang_cams.py. All row model data can be
585 obtained from the corresponding author upon request. The definitions of the regions and continents
586 used in the current analysis are based on regional masks that can be seen in Supplementary Figure
587 S 3.

588

589 Competing interests. The authors declare no competing interests.

590

591 Acknowledgements. This research was performed in the frame of the Development program of the
592 Interdisciplinary Scientific and Educational School of M. V. Lomonosov Moscow State University
593 "Future Planet and Global Environmental Change". Authors wish to thank much Dr. Tony Hanson
594 (Magee Scientific) for his support on the AE33 aethalometer installation and operation at the
595 "Island Bely" station, as well as Dr. A. Sinitsky for organizational support.

596

597 Financial support. Development of the methodology for aethalometric measurements and AAE
598 calculations was performed in the frame of RSF project #19 -77-30004. Aerosol infrastructure
599 developing methodology was implemented under the RF Ministry of Science and Higher
600 Education (agreement № 075-15-2021-938). All model and code developments and calculations
601 were supported by the COMBAT (Quantification of Global Ammonia Sources constrained by a
602 Bayesian Inversion Technique) project funded by ROMFORSK – Program for romforskning of
603 the Research Council of Norway (Project ID: 275407, website:

604 <https://prosjektbanken.forskningsradet.no/project/FORISS/275407?Kilde=FORISS&distribution=Ar&chart=bar&calcType=funding&Sprak=no&sortBy=date&sortOrder=desc&resultCount=30&offset=0&ProgAkt.3=ROMFORSK-Program+for+romforskning>) and the EC Horizon 2020 –

607 Research and Innovation Framework Programme ATMO-ACCESS Integrating Activity under
608 grant agreement No 101008004. The work was partly supported by the European Union's
609 Horizon 2020 European research infrastructures programme ACTRIS-IMP under grant
610 agreement No 871115.

611

612 Author contributions. O.B.P. supervised the station operation, interpreted data and wrote the
613 manuscript. N.E. performed all the FLEXPART simulations and analyses, wrote and coordinated
614 the paper. V.O.K. analyzed the data. M.A.C. prepared the figures and assisted in the interpretation
615 of the results. K.E. provided BB impact and AAE aging evaluation. A.G. performed AAE
616 calculations and evaluation of data quality. N.S.K. supported the research. All authors contributed
617 to the final version of the manuscript.

618

619 **References**

620

- 621 Akagi, S., Yokelson, R. J., Wiedinmyer, C., Alvarado, M., Reid, J., Karl, T., Crounse, J., and
622 Wennberg, P.: Emission factors for open and domestic biomass burning for use in atmospheric
623 models, *Atmospheric Chemistry and Physics*, 11, 4039-4072, 2011.
- 624 Andreae, M. O. and Merlet, P.: Emission of trace gases and aerosols from biomass burning,
625 *Global biogeochemical cycles*, 15, 955-966, 2001.
- 626 Bond, T. C., Doherty, S. J., Fahey, D., Forster, P., Berntsen, T., DeAngelo, B., Flanner, M.,
627 Ghan, S., Kärcher, B., and Koch, D.: Bounding the role of black carbon in the climate system: A
628 scientific assessment, *Journal of Geophysical Research: Atmospheres*, 118, 5380-5552, 2013.
- 629 Böttcher, K., Paunu, V.-V., Kupiainen, K., Zhizhin, M., Matveev, A., Savolahti, M., Klimont, Z.,
630 Väätäinen, S., Lamberg, H., and Karvosenoja, N.: Black carbon emissions from flaring in Russia
631 in the period 2012-2017, *Atmospheric Environment*, 118390, 2021.
- 632 Cappa, C. D., Kolesar, K. R., Zhang, X., Atkinson, D. B., Pekour, M. S., Zaveri, R. A.,
633 Zelenyuk, A., and Zhang, Q.: Understanding the optical properties of ambient sub- and
634 supermicron particulate matter: results from the CARES 2010 field study in northern California,
635 *Atmos. Chem. Phys.*, 16, 6511-6535, 10.5194/acp-16-6511-2016, 2016.
- 636 Cassiani, M., Stohl, A., and Brioude, J.: Lagrangian stochastic modelling of dispersion in the
637 convective boundary layer with skewed turbulence conditions and a vertical density gradient:
638 Formulation and implementation in the FLEXPART model, *Boundary-Layer Meteorology*, 154,
639 367-390, 2015.
- 640 Chang, R.-W., Leck, C., Graus, M., Müller, M., Paatero, J., Burkhardt, J. F., Stohl, A., Orr, L.,
641 Hayden, K., and Li, S.-M.: Aerosol composition and sources in the central Arctic Ocean during
642 ASCOS, *Atmospheric Chemistry and Physics*, 2011.
- 643 Cho, M.-H., Park, R. J., Yoon, J., Choi, Y., Jeong, J. I., Labzovskii, L., Fu, J. S., Huang, K.,
644 Jeong, S.-J., and Kim, B.-M.: A missing component of Arctic warming: black carbon from gas
645 flaring, *Environmental Research Letters*, 14, 094011, 2019.
- 646 Conrad, B. M. and Johnson, M. R.: Field measurements of black carbon yields from gas flaring,
647 *Environmental science & technology*, 51, 1893-1900, 2017.
- 648 Di Giuseppe, F., Remy, S., Pappenberger, F., and Wetterhall, F.: Improving CAMS biomass
649 burning estimations by means of the Global ECMWF Fire Forecast system (GEFF), ECMWF
650 Tech. Memo. 790, 18 pp., [https://www.ecmwf.int/sites/default/files ...](https://www.ecmwf.int/sites/default/files...), 2016.
- 651 Drinovec, L., Močnik, G., Zotter, P., Prévôt, A., Ruckstuhl, C., Coz, E., Rupakheti, M., Sciare,
652 J., Müller, T., and Wiedensohler, A.: The "dual-spot" Aethalometer: an improved measurement
653 of aerosol black carbon with real-time loading compensation, *Atmospheric Measurement
654 Techniques*, 8, 1965-1979, 2015.
- 655 Eckhardt, S., Quennehen, B., Olivie, D. J. L., Berntsen, T. K., Cherian, R., Christensen, J. H.,
656 Collins, W., Crepinsek, S., Daskalakis, N., Flanner, M., Herber, A., Heyes, C., Hodnebrog, Ø.,
657 Huang, L., Kanakidou, M., Klimont, Z., Langner, J., Law, K. S., Lund, M. T., Mahmood, R.,
658 Massling, A., Myriokefalitakis, S., Nielsen, I. E., Nøjgaard, J. K., Quaas, J., Quinn, P. K., Raut,
659 J. C., Rumbold, S. T., Schulz, M., Sharma, S., Skeie, R. B., Skov, H., Uttal, T., von Salzen, K.,
660 and Stohl, A.: Current model capabilities for simulating black carbon and sulfate concentrations

661 in the Arctic atmosphere: a multi-model evaluation using a comprehensive measurement data set,
662 *Atmos. Chem. Phys.*, 15, 9413-9433, 10.5194/acp-15-9413-2015, 2015.

663 Eleftheriadis, K., Vratolis, S., and Nyeki, S.: Aerosol black carbon in the European Arctic:
664 Measurements at Zeppelin station, Ny-Ålesund, Svalbard from 1998–2007, *Geophysical*
665 *Research Letters*, 36, n/a-n/a, 10.1029/2008GL035741, 2009.

666 Eleftheriadis, K., Nyeki, S., Psomiadou, C., and Colbeck, I.: Background aerosol properties in
667 the European arctic, *Water, Air and Soil Pollution: Focus*, 4, 23-30, 2004.

668 Flanner, M. G.: Arctic climate sensitivity to local black carbon, *Journal of Geophysical*
669 *Research: Atmospheres*, 118, 1840-1851, 10.1002/jgrd.50176, 2013.

670 Forrister, H., Liu, J., Scheuer, E., Dibb, J., Ziemba, L., Thornhill, K. L., Anderson, B., Diskin,
671 G., Perring, A. E., and Schwarz, J. P.: Evolution of brown carbon in wildfire plumes,
672 *Geophysical Research Letters*, 42, 4623-4630, 2015.

673 Forster, C., Stohl, A., and Seibert, P.: Parameterization of convective transport in a Lagrangian
674 particle dispersion model and its evaluation, *Journal of applied meteorology and climatology*, 46,
675 403-422, 2007.

676 Giglio, L., Randerson, J. T., and Van Der Werf, G. R.: Analysis of daily, monthly, and annual
677 burned area using the fourth-generation global fire emissions database (GFED4), *Journal of*
678 *Geophysical Research: Biogeosciences*, 118, 317-328, 2013.

679 Grange, S. K., Lötscher, H., Fischer, A., Emmenegger, L., and Hueglin, C.: Evaluation of
680 equivalent black carbon source apportionment using observations from Switzerland between
681 2008 and 2018, *Atmospheric Measurement Techniques*, 13, 1867-1885, 2020.

682 Grythe, H., Kristiansen, N. I., Groot Zwaafink, C. D., Eckhardt, S., Ström, J., Tunved, P.,
683 Krejci, R., and Stohl, A.: A new aerosol wet removal scheme for the Lagrangian particle model
684 FLEXPART v10, *Geosci. Model Dev.*, 10, 1447-1466, 10.5194/gmd-10-1447-2017, 2017.

685 Helin, A., Virkkula, A., Backman, J., Pirjola, L., Sippula, O., Aakko-Saksa, P., Väätäinen, S.,
686 Mylläri, F., Järvinen, A., and Bloss, M.: Variation of absorption Ångström exponent in aerosols
687 from different emission sources, *Journal of Geophysical Research: Atmospheres*, 126,
688 e2020JD034094, 2021.

689 Huang, K., Fu, J. S., Prikhodko, V. Y., Storey, J. M., Romanov, A., Hodson, E. L., Cresko, J.,
690 Morozova, I., Ignatieva, Y., and Cabaniss, J.: Russian anthropogenic black carbon: Emission
691 reconstruction and Arctic black carbon simulation, *Journal of Geophysical Research:*
692 *Atmospheres*, 120, 11,306-311,333, 2015.

693 Ismail, O. S. and Umukoro, G. E.: Global impact of gas flaring, *Energy and Power Engineering*,
694 4, 290, 2012.

695 Johnson, M. S., Strawbridge, K., Knowland, K. E., Keller, C., and Travis, M.: Long-range
696 transport of Siberian biomass burning emissions to North America during FIREX-AQ,
697 *Atmospheric Environment*, 252, 118241, 2021.

698 Kaiser, J., Heil, A., Andreae, M., Benedetti, A., Chubarova, N., Jones, L., Morcrette, J.-J.,
699 Razinger, M., Schultz, M., and Suttie, M.: Biomass burning emissions estimated with a global
700 fire assimilation system based on observed fire radiative power, *Biogeosciences*, 9, 527-554,
701 2012.

702 Kalogridis, A.-C., Vratolis, S., Liakakou, E., Gerasopoulos, E., Mihalopoulos, N., and
703 Eleftheriadis, K.: Assessment of wood burning versus fossil fuel contribution to wintertime black
704 carbon and carbon monoxide concentrations in Athens, Greece, *Atmospheric Chemistry and*
705 *Physics*, 18, 10219-10236, 2018a.

706 Kalogridis, A. C., Popovicheva, O. B., Engling, G., Diapouli, E., Kawamura, K., Tachibana, E.,
707 Ono, K., Kozlov, V. S., and Eleftheriadis, K.: Smoke aerosol chemistry and aging of Siberian
708 biomass burning emissions in a large aerosol chamber, *Atmospheric Environment*, 185, 15-28,
709 <https://doi.org/10.1016/j.atmosenv.2018.04.033>, 2018b.

710 Kaufman, Y., Ichoku, C., Giglio, L., Korontzi, S., Chu, D., Hao, W., Li, R.-R., and Justice, C.:
711 Fire and smoke observed from the Earth Observing System MODIS instrument--products,
712 validation, and operational use, *International Journal of Remote Sensing*, 24, 1765-1781, 2003.

713 Klimont, Z., Kupiainen, K., Heyes, C., Purohit, P., Cofala, J., Rafaj, P., Borcken-Kleefeld, J., and
714 Schöpp, W.: Global anthropogenic emissions of particulate matter including black carbon,
715 Atmospheric Chemistry and Physics Discussions, 17, 8681-8723, 2017.

716 Kozlov, V. S., Panchenko, M. V., Shmargunov, V. P., Chernov, D. G., Yausheva, E. P., Pol'kin,
717 V. V., and Terpugova, S. A.: Long-term investigations of the spatiotemporal variability of black
718 carbon and aerosol concentrations in the troposphere of West Siberia and Russian Subarctic,
719 Химия в интересах устойчивого развития, 24, 423-440, 2016.

720 Long, C. M., Nascarella, M. A., and Valberg, P. A.: Carbon black vs. black carbon and other
721 airborne materials containing elemental carbon: Physical and chemical distinctions,
722 Environmental Pollution, 181, 271-286, 2013.

723 Manousakas, M., Popovicheva, O., Evangeliou, N., Diapouli, E., Sitnikov, N., Shonija, N., and
724 Eleftheriadis, K.: Aerosol carbonaceous, elemental and ionic composition variability and origin
725 at the Siberian High Arctic, Cape Baranova, Tellus B: Chemical and Physical Meteorology, 72,
726 1-14, 2020.

727 Paris, J.-D., Stohl, A., Nédélec, P., Arshinov, M. Y., Panchenko, M., Shmargunov, V., Law, K.
728 S., Belan, B., and Ciais, P.: Wildfire smoke in the Siberian Arctic in summer: source
729 characterization and plume evolution from airborne measurements, Atmospheric Chemistry and
730 Physics, 9, 9315-9327, 2009.

731 Pisso, I., Sollum, E., Grythe, H., Kristiansen, N. I., Cassiani, M., Eckhardt, S., Arnold, D.,
732 Morton, D., Thompson, R. L., and Groot Zwaaftink, C. D.: The Lagrangian particle dispersion
733 model FLEXPART version 10.4, Geoscientific Model Development, 12, 4955-4997, 2019.

734 Popovicheva, O., Chichaeva, M., Kobelev, V., Sinitskiy, A., and Hansen, A.: Black Carbon in
735 urban emissions on the Polar Circle, 26th International Symposium on Atmos. Ocean Optics,
736 Proc. SPIE, 11560J,

737 Popovicheva, O., Timofeev, M., Persiantseva, N., Jefferson, M. A., Johnson, M., Rogak, S. N.,
738 and Baldelli, A.: Microstructure and chemical composition of particles from small-scale gas
739 flaring, Aerosol and Air Quality Research, 19, 2205-2221, 2019a.

740 Popovicheva, O., Diapouli, E., Makshtas, A., Shonija, N., Manousakas, M., Saraga, D., Uttal, T.,
741 and Eleftheriadis, K.: East Siberian Arctic background and black carbon polluted aerosols at
742 HMO Tiksi, Science of the Total Environment, 655, 924-938, 2019b.

743 Popovicheva, O. B., Evangeliou, N., Eleftheriadis, K., Kalogridis, A. C., Sitnikov, N., Eckhardt,
744 S., and Stohl, A.: Black Carbon Sources Constrained by Observations in the Russian High
745 Arctic, Environmental Science & Technology, 51, 3871-3879, 10.1021/acs.est.6b05832, 2017.

746 Qi, L. and Wang, S.: Sources of black carbon in the atmosphere and in snow in the Arctic,
747 Science of The Total Environment, 691, 442-454, 2019.

748 Quinn, P. K., Bates, T. S., Baum, E., Doubleday, N., Fiore, A. M., Flanner, M., Fridlind, A.,
749 Garrett, T. J., Koch, D., Menon, S., Shindell, D., Stohl, A., and Warren, S. G.: Short-lived
750 pollutants in the Arctic: their climate impact and possible mitigation strategies, Atmos. Chem.
751 Phys., 8, 1723-1735, 10.5194/acp-8-1723-2008, 2008.

752 Randerson, J., Chen, Y., Van Der Werf, G., Rogers, B., and Morton, D.: Global burned area and
753 biomass burning emissions from small fires, Journal of Geophysical Research: Biogeosciences,
754 117, 2012.

755 Ren, L., Yang, Y., Wang, H., Zhang, R., Wang, P., and Liao, H.: Source attribution of Arctic
756 black carbon and sulfate aerosols and associated Arctic surface warming during 1980–2018,
757 Atmospheric Chemistry and Physics, 20, 9067-9085, 2020.

758 Romshoo, B., Müller, T., Pfeifer, S., Saturno, J., Nowak, A., Ciupek, K., Quincey, P., and
759 Wiedensohler, A.: Optical properties of coated black carbon aggregates: numerical simulations,
760 radiative forcing estimates, and size-resolved parameterization scheme, Atmos. Chem. Phys., 21,
761 12989-13010, 10.5194/acp-21-12989-2021, 2021.

762 Saleh, R., Hennigan, C., McMeeking, G., Chuang, W., Robinson, E., Coe, H., Donahue, N., and
763 Robinson, A.: Absorptivity of brown carbon in fresh and photo-chemically aged biomass-
764 burning emissions, Atmospheric Chemistry and Physics, 13, 7683-7693, 2013.

765 Sandradewi, J., Prévôt, A. S., Szidat, S., Perron, N., Alfarra, M. R., Lanz, V. A., Weingartner, E.,
766 and Baltensperger, U.: Using aerosol light absorption measurements for the quantitative
767 determination of wood burning and traffic emission contributions to particulate matter,
768 *Environmental science & technology*, 42, 3316-3323, 2008.

769 Schacht, J., Heinold, B., Quaas, J., Backman, J., Cherian, R., Ehrlich, A., Herber, A., Huang, W.
770 T. K., Kondo, Y., Massling, A., Sinha, P. R., Weinzierl, B., Zanatta, M., and Tegen, I.: The
771 importance of the representation of air pollution emissions for the modeled distribution and
772 radiative effects of black carbon in the Arctic, *Atmos. Chem. Phys.*, 19, 11159-11183,
773 10.5194/acp-19-11159-2019, 2019.

774 Sharma, S., Lavoué, D., Cachier, H., Barrie, L., and Gong, S.: Long-term trends of the black
775 carbon concentrations in the Canadian Arctic, *Journal of Geophysical Research: Atmospheres*,
776 109, 2004.

777 Stathopoulos, V., Evangeliou, N., Stohl, A., Vratolis, S., Matsoukas, C., and Eleftheriadis, K.:
778 Large circulation patterns strongly modulate long term variability of Arctic black carbon levels
779 and areas of origin, *Geophysical Research Letters*, e2021GL092876, 2021.

780 Stohl, A.: Characteristics of atmospheric transport into the Arctic troposphere, *Journal of*
781 *Geophysical Research: Atmospheres*, 111, n/a-n/a, 10.1029/2005JD006888, 2006.

782 Stohl, A., Forster, C., Frank, A., Seibert, P., and Wotawa, G.: Technical note: The Lagrangian
783 particle dispersion model FLEXPART version 6.2, *Atmos. Chem. Phys.*, 5, 2461-2474,
784 10.5194/acp-5-2461-2005, 2005.

785 Stohl, A., Klimont, Z., Eckhardt, S., Kupiainen, K., Shevchenko, V. P., Kopeikin, V. M., and
786 Novigatsky, A. N.: Black carbon in the Arctic: the underestimated role of gas flaring and
787 residential combustion emissions, *Atmos. Chem. Phys.*, 13, 8833-8855, 10.5194/acp-13-8833-
788 2013, 2013.

789 Stohl, A., Andrews, E., Burkhardt, J., Forster, C., Herber, A., Hoch, S., Kowal, D., Lunder, C.,
790 Mefford, T., and Ogren, J.: Pan-Arctic enhancements of light absorbing aerosol concentrations
791 due to North American boreal forest fires during summer 2004, *Journal of Geophysical*
792 *Research: Atmospheres*, 111, 2006.

793 Stohl, A., Berg, T., Burkhardt, J., Fjæraa, A., Forster, C., Herber, A., Hov, Ø., Lunder, C.,
794 McMillan, W., and Oltmans, S.: Arctic smoke—record high air pollution levels in the European
795 Arctic due to agricultural fires in Eastern Europe in spring 2006, *Atmospheric Chemistry and*
796 *Physics*, 7, 511-534, 2007.

797 Stone, R. S., Sharma, S., Herber, A., Eleftheriadis, K., and Nelson, D. W.: A characterization of
798 Arctic aerosols on the basis of aerosol optical depth and black carbon measurements, *Elem Sci*
799 *Anth*, 2, 2014.

800 Treffeisen, R., Turnved, P., Ström, J., Herber, A., Bareiss, J., Helbig, A., Stone, R. S.,
801 Hoyningen-Huene, W., Krejci, R., Stohl, A., and Neuber, R.: Arctic smoke ? aerosol
802 characteristics during a record air pollution event in the European Arctic and its radiative impact,
803 *Atmospheric Chemistry and Physics Discussions*, 7, 2275-2324, 2007.

804 Tunved, P., Ström, J., and Krejci, R.: Arctic aerosol life cycle: linking aerosol size distributions
805 observed between 2000 and 2010 with air mass transport and precipitation at Zeppelin station,
806 Ny-Å lesund, Svalbard, *Atmospheric Chemistry & Physics*, 13, 3643-3660, 2013.

807 Vinogradova, A.: Anthropogenic Black Carbon emissions to the atmosphere: surface distribution
808 through Russian territory, *Atmospheric and Oceanic Optics*, 28, 158-164, 2015.

809 Virkkula, A.: Modeled source apportionment of black carbon particles coated with a light-
810 scattering shell, *Atmospheric Measurement Techniques*, 14, 3707-3719, 2021.

811 Voronova, O., Zima, A., Kladov, V., and Cherepanova, E.: Anomalous Wildfires in Siberia in
812 Summer 2019, *Izvestiya, Atmospheric and Oceanic Physics*, 56, 1042-1052, 2020.

813 Wang, Q., Jacob, D. J., Fisher, J. A., Mao, J., Leibensperger, E. M., Carouge, C. C., Le Sager, P.,
814 Kondo, Y., Jimenez, J. L., Cubison, M. J., and Doherty, S. J.: Sources of carbonaceous aerosols
815 and deposited black carbon in the Arctic in winter-spring: implications for radiative forcing,
816 *Atmos. Chem. Phys.*, 11, 12453-12473, 10.5194/acp-11-12453-2011, 2011.

817 Warneke, C., Froyd, K., Brioude, J., Bahreini, R., Brock, C., Cozic, J., De Gouw, J., Fahey, D.,
818 Ferrare, R., and Holloway, J.: An important contribution to springtime Arctic aerosol from
819 biomass burning in Russia, *Geophysical Research Letters*, 37, 2010.

820 Werf, G. R., Randerson, J. T., Giglio, L., Leeuwen, T. T. v., Chen, Y., Rogers, B. M., Mu, M.,
821 Van Marle, M. J., Morton, D. C., and Collatz, G. J.: Global fire emissions estimates during
822 1997–2016, *Earth System Science Data*, 9, 697-720, 2017.

823 Winiger, P., Andersson, A., Eckhardt, S., Stohl, A., and Gustafsson, Ö.: The sources of
824 atmospheric black carbon at a European gateway to the Arctic, *Nature communications*, 7, 1-8,
825 2016.

826 Winiger, P., Andersson, A., Eckhardt, S., Stohl, A., Semiletov, I. P., Dudarev, O. V., Charkin,
827 A., Shakhova, N., Klimont, Z., Heyes, C., and Gustafsson, Ö.: Siberian Arctic black carbon
828 sources constrained by model and observation, *Proceedings of the National Academy of
829 Sciences*, 114, E1054-E1061, 10.1073/pnas.1613401114, 2017.

830 Wooster, M. J., Roberts, G., Perry, G., and Kaufman, Y.: Retrieval of biomass combustion rates
831 and totals from fire radiative power observations: FRP derivation and calibration relationships
832 between biomass consumption and fire radiative energy release, *Journal of Geophysical
833 Research: Atmospheres*, 110, 2005.

834 Yun, Y., Penner, J. E., and Popovicheva, O.: The effects of hygroscopicity on ice nucleation of
835 fossil fuel combustion aerosols in mixed-phase clouds, *Atmos. Chem. Phys.*, 13, 4339-4348,
836 10.5194/acp-13-4339-2013, 2013.

837 Zhu, C., Kanaya, Y., Takigawa, M., Ikeda, K., Tanimoto, H., Taketani, F., Miyakawa, T.,
838 Kobayashi, H., and Pisso, I.: FLEXPART v10. 1 simulation of source contributions to Arctic
839 black carbon, *Atmospheric Chemistry and Physics*, 20, 1641-1656, 2020.

840 Zotter, P., Herich, H., Gysel, M., El-Haddad, I., Zhang, Y., Močnik, G., Hüglin, C.,
841 Baltensperger, U., Szidat, S., and Prévôt, A. S.: Evaluation of the absorption Ångström
842 exponents for traffic and wood burning in the Aethalometer-based source apportionment using
843 radiocarbon measurements of ambient aerosol, *Atmospheric Chemistry and Physics*, 17, 4229-
844 4249, 2017.

845

846

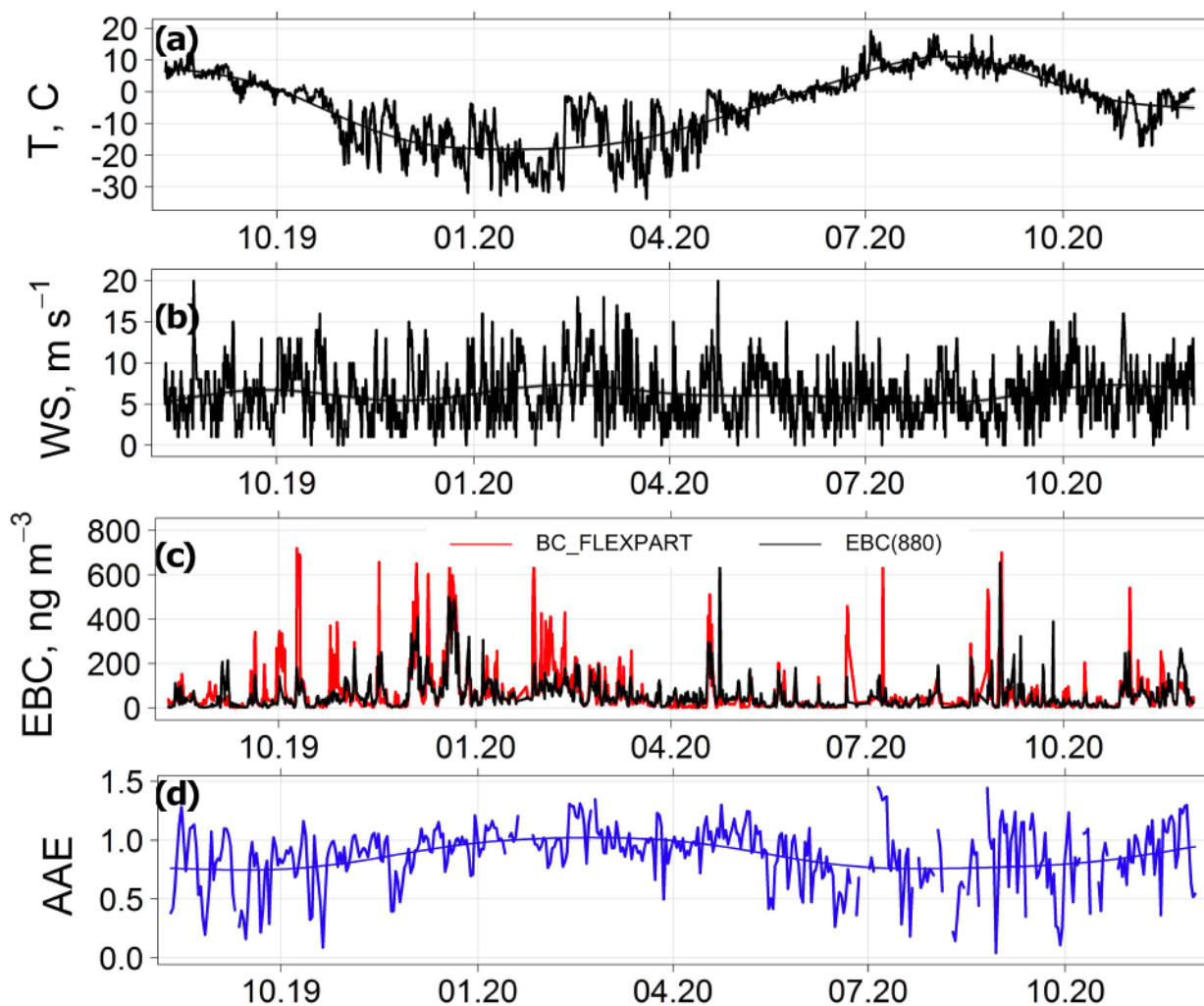
848



849

850 **Figure 1.** Top left map shows the location of the newly established “Island Bely” aerosol station
 851 in contrast to other Arctic stations (Zeppelin, Alert, Barrow, Summit, Tiksi, and Cape Baranova).
 852 Bottom left map shows a zoomed version of the location of the Bely Island in the Kara Sea, where
 853 the new station was developed (73°20'7.57"N, 70°4'49.05"E). The map on the right shows the
 854 “Island Bely” aerosol station in combination with the European part of Russia and Western Siberia
 855 and the Yamalo-Nenets Autonomous Okrug (YNAO). Flares of oil and gas fields are shown for
 856 2019 year in brown triangles (adopted from <https://skytruth.org/>).

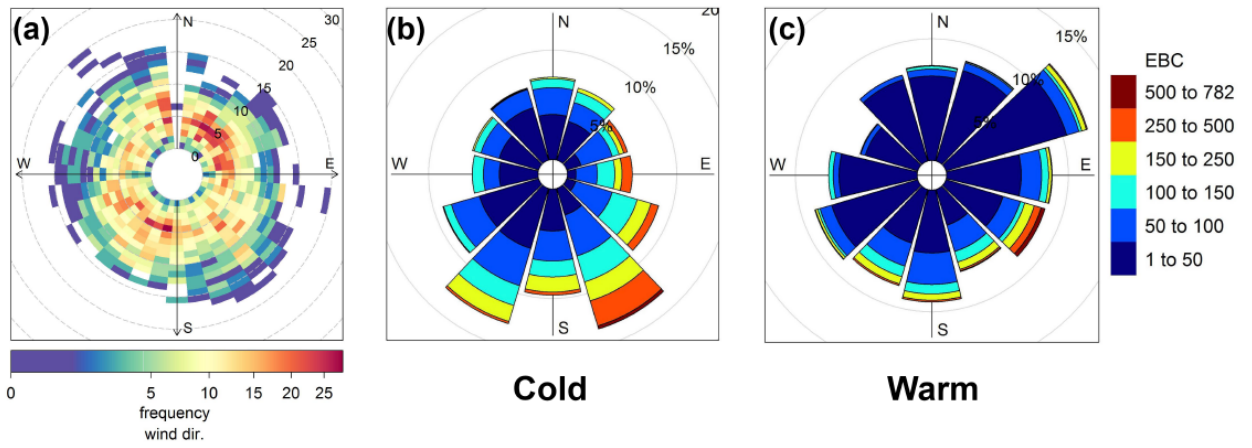
857



858

859 **Figure 2.** Meteorological conditions with respect to (a) mean temperature and (b) wind speed (data
 860 were smoothed to show long-term variations), (c) time-series of 24-h median EBC (black) and
 861 model BC using ECLIPSEv6 - CAMS emissions (red), and (d) 24-h average Absorption Ångström
 862 Exponent (AAE) measured at “Island Bely” station from 10 August 2019 to 30 November 2020
 863 (date format in mm.yy).

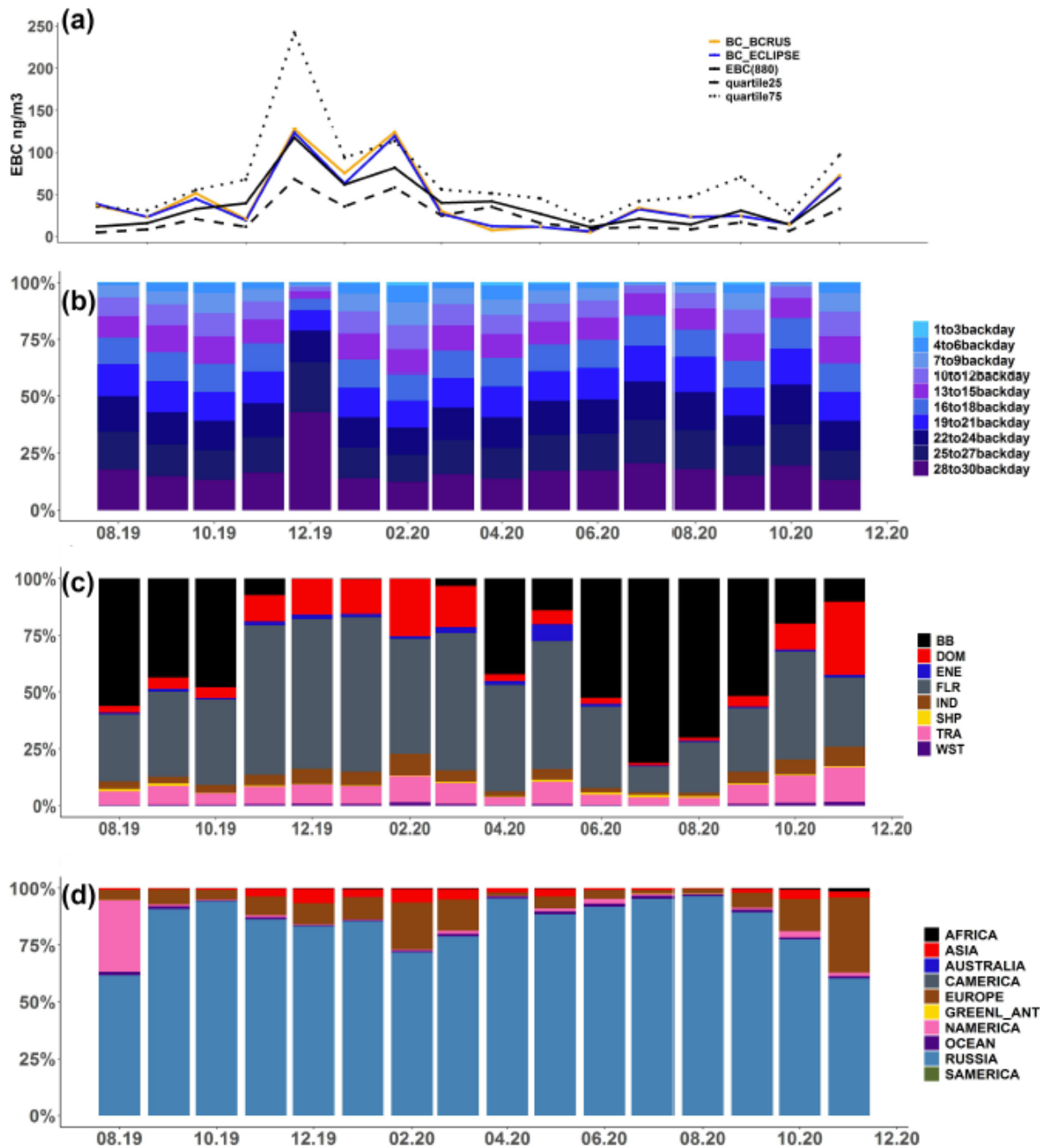
864



865

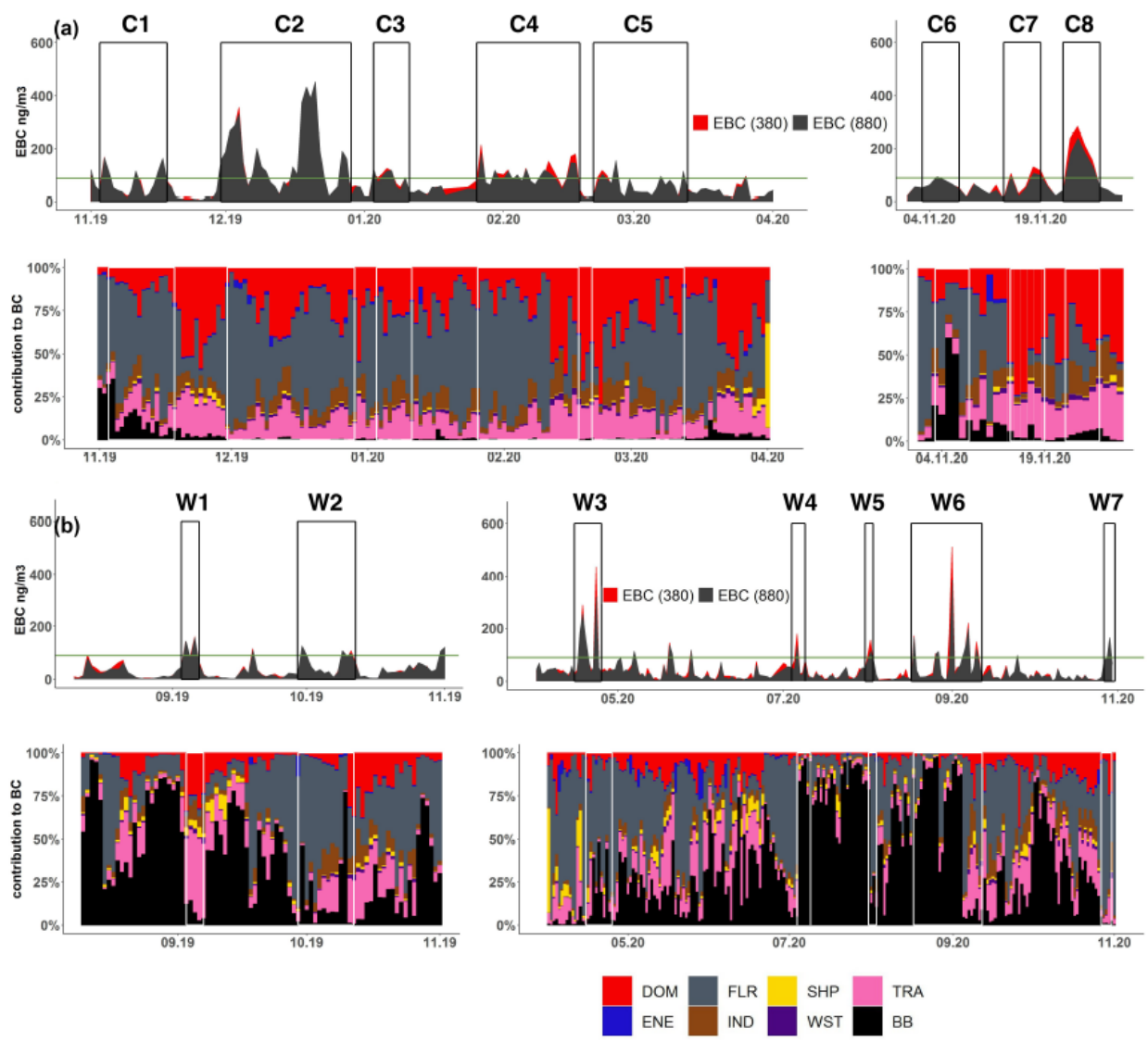
866 **Figure 3.** (a) Polar frequency plots of wind speed and direction. Each cell gives the total number
 867 of hours the wind was originating from a certain wind direction. The dashed circular grey lines
 868 show the wind speed (in m s^{-1}). Rose diagrams show 3h EBC concentrations during the cold (b)
 869 and warm (c) periods.

870



871

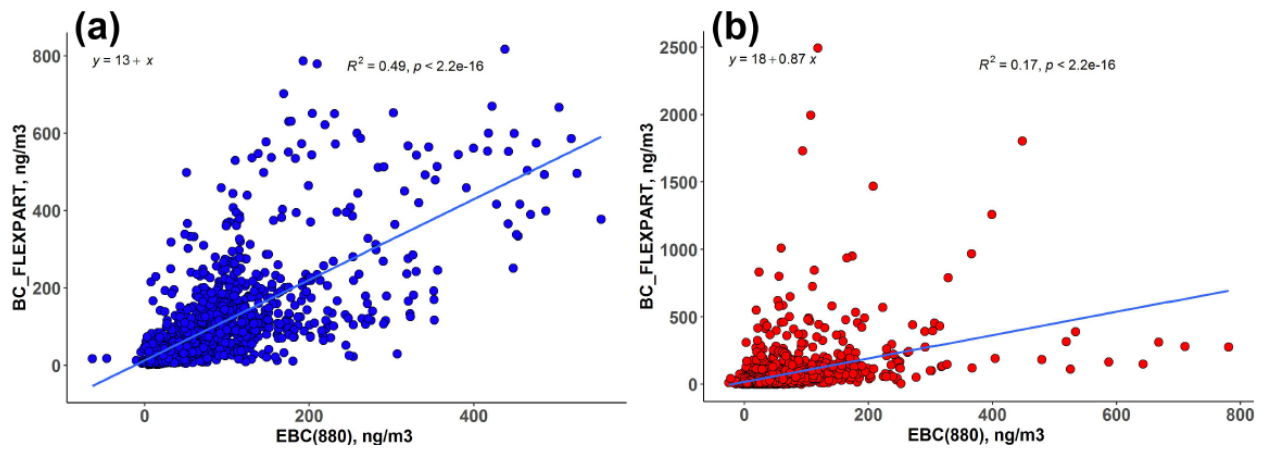
872 **Figure 4.** (a) Monthly climatology of EBC at the “Island Bely” station depicting medians, 25th and
 873 75th percentiles (dashed lines). Near-surface monthly median BC concentrations simulated with
 874 FLEXPART coupled to ECLIPSEv6-CAMS (steel blue) and ECLIPSEv6-BCRUS-CAMS (red)
 875 emissions are also shown. (b) Age spectrum of modelled BC from all possible sources showing
 876 the contribution of emissions from each day back in time to the surface concentration of BC. (c)
 877 Contribution from different emission source types to surface BC concentrations. The emission
 878 sources of biomass burning (BB) adopted from GFEDv4.1, and residential and commercial
 879 (DOM), power plants, energy conversion, and extraction (ENE), gas flaring (FLR), industrial
 880 combustion and processing (IND), shipping (SHP), and transportation (TRA) adopted from
 881 ECLIPSEv6 were considered. (d) Continental spectrum showing the contribution from each
 882 continent or region to surface BC concentrations . 10 regions were considered namely, Africa,
 883 Asia, Australia, Central America, Europe, Greenland/Antarctica, North America, World Ocean,
 884 Russia, and South America (see Supplementary Figure S 3).



885

886 **Figure 5.** 24-h median EBC concentrations measured at 880 nm (black) and 370 nm (red), and
 887 source contributions to surface BC from anthropogenic (DOM, ENE, FLR, IND, SHP, WST,
 888 TRA) and BB sources for (a) the cold and (b) the warm period. Pollution episodes were composed
 889 from the periodically repeated events of high EBC concentration. The green straight line indicates
 890 the pollution level of the 80th percentile.

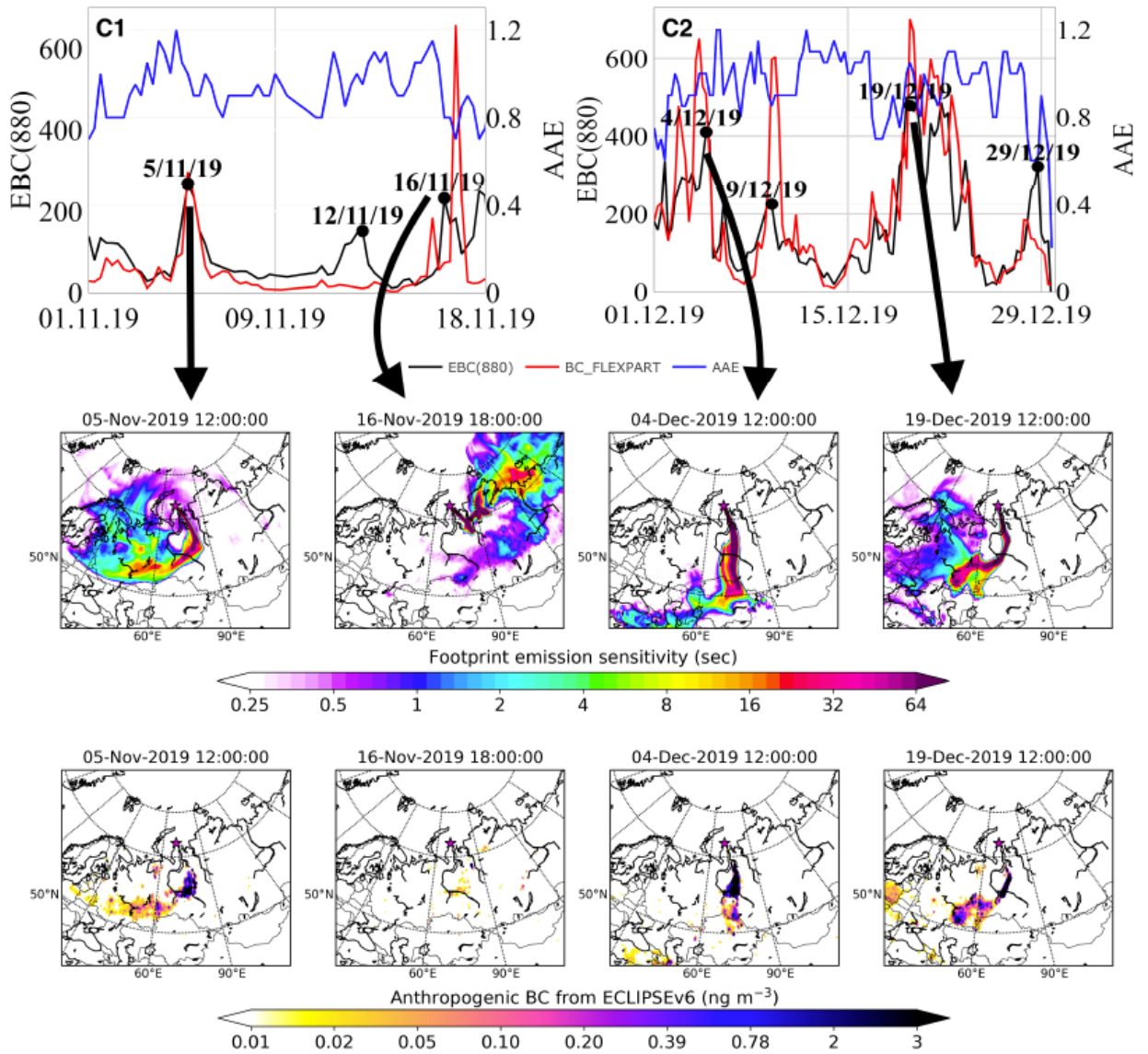
891



892

893 **Figure 6.** Scatter-plots of 3-h median measured EBC (880) against modelled BC from
 894 FLEXPART for the (a) cold and (b) warm period. Solid line is the linear regression fit of the
 895 comparison between modelled and observed values.

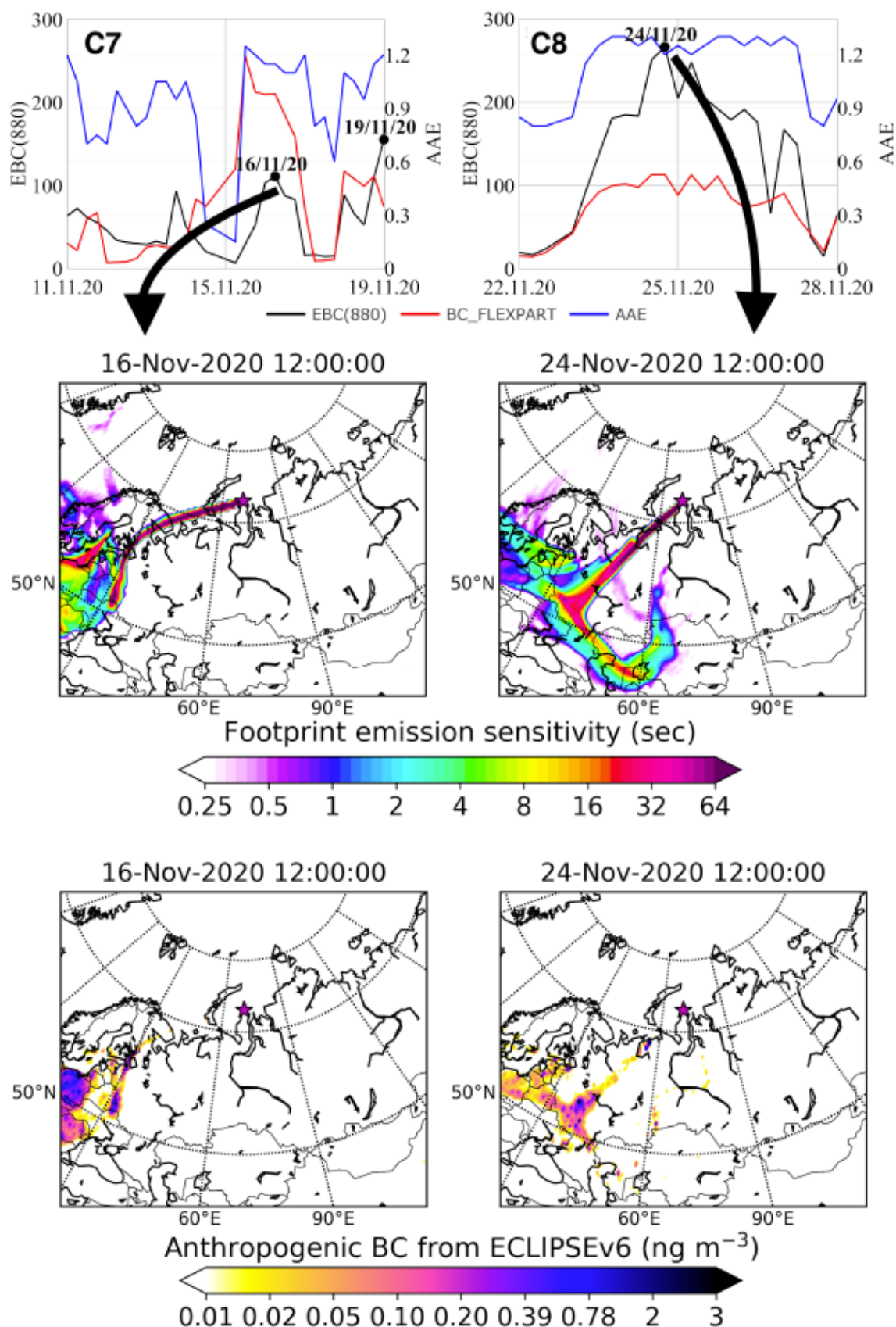
896



898

899 **Figure 7.** Examples of pollution episodes C1 and C2 observed in the cold period (see **Figure 5a**),
 900 where FLR contribution prevails. 6-h median EBC (880) (black line), BC simulated with
 901 FLEXPART (red line), AAE (blue line) (upper row). Footprint emissions sensitivities in seconds
 902 showing the largest probability of emission origin (middle row). Spatial distribution of
 903 anthropogenic contribution (in ng/m³) to surface BC at the “Island Bely” station (bottom row).

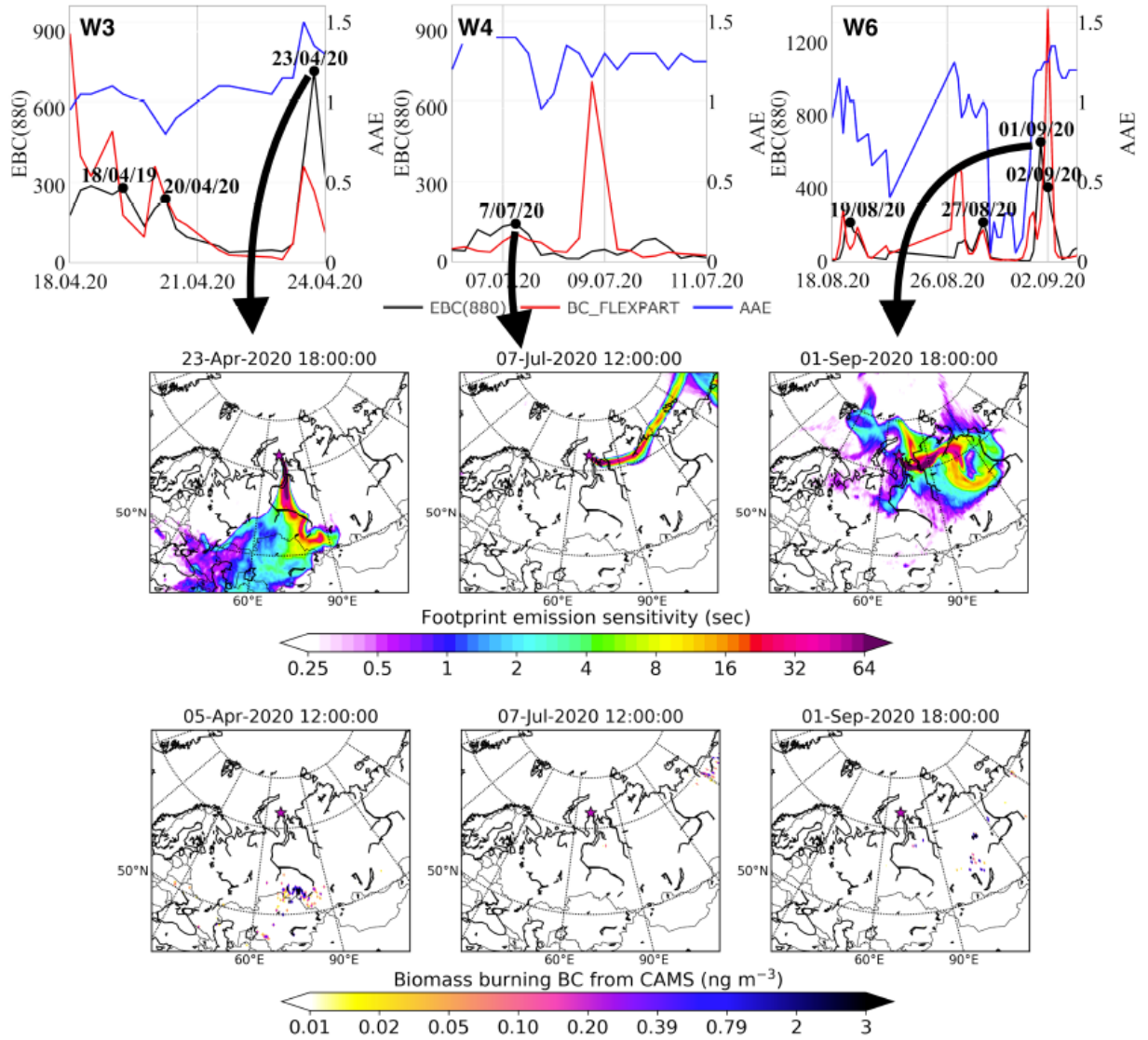
904



905

906 **Figure 8.** Examples of pollution episodes C7 and C8 observed in the cold period (see **Figure 5a**),
 907 where DOM and TRA contribution prevails. Timeseries of measured EBC, modelled BC and AAE
 908 (upper row), footprint emissions sensitivities (middle row) and anthropogenic contribution to
 909 surface BC (bottom row) are shown.

910



911

912 **Figure 9.** Examples of pollution episodes W3, W4 and W6 in the warm period (see **Figure 5b**),
913 where BB contribution prevails. The figure has been arranged similar to **Figure 7** (timeseries of
914 measured EBC, modelled BC and AAE, footprint emissions sensitivities and BB contribution to
915 surface BC).

916